# PAPER C

# ANISOTROPIC TOMOGRAPHY

**Reinaldo J. Michelena and Jerry M. Harris**
*Seismic Tomography Project*

## ABSTRACT

Tomographic estimation of velocities is usually performed by fitting picked traveltime data to a set of time/distance equations using a slowness function which is not dependent on angle. If the medium is assumed to be transversely isotropic with vertical symmetry axis, an elliptic form can be used to approximate the traveltime-distance relationship. When this relationship is used to fit the data, the result is two images representing the vertical and horizontal components of slowness. The inversion is a simple extension of the well known isotropic schemes and whether it is successful depends on the range of ray angles available. This is illustrated with synthetic and field-data examples.

## INTRODUCTION

Depending on the degree of anisotropy of the medium and the seismic wavelengths used, the tomograms obtained from cross-well traveltime data assuming that the medium is isotropic may suffer from severe distortions. These distortions are analogous to the well known mispositions occurred in surface seismic when, in an anisotropic environment, the stacking velocity is used to control depth conversion. Eliminating these distortions is one reason to allow the model to be anisotropic in tomographic traveltime inversion. If we do that, we are not only solving an imaging problem. It is well known that anisotropy can be a useful tool for studying lithology and degree of stratification in sedimentary rocks and therefore, taking into account velocity anisotropy in tomographic traveltime inversion also helps to gain extra and useful information about the reservoir.

From surface seismic measurements, whether reflection or refraction, it is possible to obtain the horizontal component of the slowness. However, for estimating anisotropy, additional subsurface information (layer thicknesses or vertical slownesses) is required (Levin, 1978). For this reason, in recent studies where anisotropy has been quantified, either a different geometry like VSP has been used (Byun and Corrigan, 1990; White et al., 1983) or the surface seismic information has been combined with well-logs (Banik, 1984). However, based on the observation that velocity anisotropy does not affect $P$-wave moveout considerably, Winterstein (1986) estimated the required layer thicknesses using velocities obtained form $P$-wave velocity analysis and

then, from *SH*-wave velocity analysis, he was able to estimate velocity anisotropy. Dellinger (1989) concludes that because of the ill-conditioning of the problem, it is not possible to estimate with high accuracy a 2-D vector velocity field from VSP-like geometries.

From cross-well measurements, fewer attempts have been made to estimate velocity anisotropy. Karrenbach (1989) proposes a practical scheme for estimating velocity and $Q$ in homogeneous transversely isotropic media, fitting elliptical curves to the dispersion relations. Cunha-Filho (1990) fits elliptical curves in layered models to cross-well traveltimes. Chapman and Pratt (1990) and Pratt and Chapman (1990) estimate velocity anisotropy in a general 2-D medium assuming, in contrast with the works of Karrenbach and Cunha-Filho, weak anisotropy. This allows the ray tracing to be performed in isotropic media.

The main difference between tomographic velocity estimation from surface measurements and cross-well measurements is that the former requires to know a priori the depths of the reflectors whereas the later does not. The only positions needed to estimate velocities from cross-well traveltimes are the source-receiver locations. When sources and receivers are located at depth, the cross-well configuration eliminates one non-linearity of the tomographic inversion of reflection traveltimes: unknown positions of reflectors. By eliminating this non-linearity, the estimation of other non-linear effects in the traveltimes, such as velocity anisotropy, should be simpler when cross-well traveltimes are used.

In this paper we present a tomographic technique to estimate velocity anisotropy if the medium is transversely isotropic with vertical symmetry axis. The technique presented here generalizes the idea of tomographic inversion in isotropic media (McMechan, 1983) where the model is discretized into orthogonal regions and the Jacobian is related to the intersection of the rays with all those regions. Instead of using a circular relationship between time and distance, we assume an elliptical relation. Both components of the slowness are estimated *simultaneously*, without using any additional information.

When fitting ellipses to the traveltimes we obtain: $S_x$ and $S_{znmo}$ (for cross-well geometries) and $S_{xnmo}$ and $S_z$ (for VSP-like geometries). In the previous notation, "*nmo*" highlights the slownesses poorly sampled by the corresponding recording geometry. These slownesses do not necessarily correspond to the true slownesses of the medium. However, they can be used to estimate the real slowness surface using an approximate expression derived by Muir (1990).

We study the effects of the limited view of the measurements (from cross-well geometries) in the estimation of both slowness components. We conclude that our technique is stable when used to invert 1-D (layered) models if the range of ray angles is "wide enough". In 2-D models, the estimation of lateral variations in the vertical component of the slowness is particularly difficult from cross-well geometries alone. Consequently, spatial variations in velocity anisotropy cannot be estimated at the same scale of variations in velocity.

The theory presented in the first part of the paper is illustrated with synthetic examples and applications to field data from a cross-well geometry.

## FORWARD MODELING

We start by defining the equations needed to do the forward modeling step in the inversion algorithm. In an homogeneous transversely isotropic media, the traveltime between two different points separated by a distance $l = \sqrt{\Delta x^2 + \Delta z^2}$ can be expressed as

$$t = \sqrt{\Delta x^2 S_x^2 + \Delta z^2 S_z^2} \tag{1a}$$

or

$$t^2 = \Delta x^2 S_x^2 + \Delta z^2 S_z^2, \tag{1b}$$

where $S_x$ and $S_z$ are the horizontal and vertical slownesses respectively. Since the medium is homogeneous, the ray path is straight.

An heterogeneous medium can be approximated as a superposition of non-overlapping homogeneous regions. For this medium, the previous expression for the traveltime between two points can be easily generalized as follows:

$$\begin{aligned} t_i &= \sum_{j=1}^{N} \sqrt{\Delta x_{ij}^2 S_{x_j}^2 + \Delta z_{ij}^2 S_{z_j}^2} \qquad i = 1, ..., M, \\ &= \sum_{j=1}^{N} t_{ij} \end{aligned} \tag{2}$$

where $t_{ij}$ is the traveltime of the $i^{th}$ ray in the $j^{th}$ cell and $S_{x_j}$ and $S_{z_j}$ are the horizontal and vertical slownesses respectively in that cell. $\Delta x_{ij}$ and $\Delta z_{ij}$ are the horizontal and vertical distances traveled by the $i^{th}$ ray in each cell. If the slowness contrasts among adjacent cells are small, the ray paths can be approximated by straight lines. In equation (2), $N$ is the total number of cells and $M$ is the total number of traveltimes.

The slowness model can be seen as a vector $\boldsymbol{S}$ whose components contain the horizontal and vertical slownesses of each cell. This vector can be defined as follows:

$$S_i = S_{x_i} \tag{3a}$$

$$S_{i+N} = S_{z_i}. \tag{3b}$$

Then, the slowness vector $\boldsymbol{S}$ has the following form:

$$\boldsymbol{S} = (S_1, S_2, \ldots, S_N, S_{N+1}, S_{N+2}, S_{N+3}, \ldots, S_{2N})^T \tag{4}$$

where $T$ means transpose. The first $N$ components correspond to the horizontal slownesses of all the cells and the second $N$ components correspond to the vertical slownesses. When the model is homogeneous, $\boldsymbol{S}$ is 2-dimensional and in general, for an heterogeneous model described by $N$ cells, $\boldsymbol{S}$ is $2N$-dimensional. Figure 1 shows the vector $\boldsymbol{S}$ for the particular case of a layered medium.

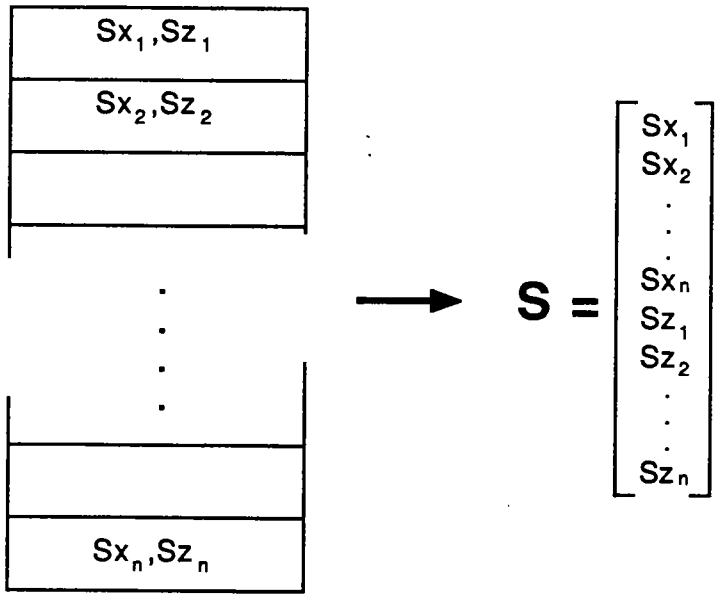


Figure 1: Slowness vector in a layered medium. (S-in-layers) [R]

Using the new variables introduced in (3), the traveltime equation (2) can be written as

$$t_i \;=\; t_i(\boldsymbol{S}) \;=\; \sum_{j=1}^{N} \sqrt{\Delta x_{ij}{}^2 S_j^2 + \Delta z_{ij}{}^2 S_{j+N}^2}. \tag{5}$$

Notice that when the medium is isotropic ($S_j = S_{j+N}$), equation (5) reduces to the familiar equation that approximates the traveltimes computed in an isotropic model described by cells (McMechan, 1983):

$$\begin{aligned} t_i \;&=\; \sum_{j=1}^{N} S_j \sqrt{\Delta x_{ij}{}^2 + \Delta z_{ij}{}^2} \\ &=\; \sum_{j=1}^{N} S_j l_{ij} \end{aligned} \tag{6}$$

where $l_{ij}$ is the length of the $i^{th}$ ray in the $j^{th}$ cell.

In the next section we will see that when expression (5) is linearized, it can be used for estimating the horizontal and vertical slownesses in an heterogeneous anisotropic model given a set of traveltimes measurements from a cross-well configuration. Equation (5) can also be used for surface geometries, as long as the depths of the reflectors are known a priori.

## INVERSE MODELING

As mentioned above, expression (5) will be used to estimate the $2N$-dimensional slowness vector $\boldsymbol{S}$ given the traveltimes from a cross-well experiment. However, we can investigate some of the difficulties in estimating such a vector by first studying the case of a homogeneous medium ($N = 1$)

When the model is isotropic, we usually estimate the slowness $S$ of the homogeneous medium that best fits the traveltimes by simply averaging all the slownesses $S_i$ obtained from the individual rays:

$$S = \frac{1}{M}\sum_{i=1}^{M} S_i = \frac{1}{M}\sum_{i=1}^{M} \frac{t_i}{l_i}, \tag{7}$$

where $l_i$ is the source-receiver distance and $M$ the total number of traveltimes.

When the model is anisotropic, the 2-D vector $\boldsymbol{S}$ that best fit the traveltimes can be obtained by generalizing the average (7). This generalization is, as expected, in a least-squares sense. Note that expression (1b) is linear in $S_x^2$ and $S_z^2$. Therefore, for a given set of traveltimes and source-receiver locations, it is possible to set up a least-squares problem to find the vector $\boldsymbol{S}$ of the homogeneous medium. Defining $W_x = S_x^2$ and $W_z = S_z^2$, the least-squares problem is

$$\underset{\sim}{\mathbf{M}} \begin{pmatrix} W_x \\ W_z \end{pmatrix} = \boldsymbol{d}, \tag{8}$$

where

$$\underset{\sim}{\mathbf{M}} = \begin{pmatrix} {\Delta x_1}^2 & {\Delta z_1}^2 \\ {\Delta x_2}^2 & {\Delta z_2}^2 \\ \vdots & \vdots \\ {\Delta x_M}^2 & {\Delta z_M}^2 \end{pmatrix},$$

and

$$\boldsymbol{d} = \begin{pmatrix} t_1^2 \\ t_2^2 \\ \vdots \\ t_M^2 \end{pmatrix}.$$

Equation (8) can be solved in different ways. The most popular approach is by using the normal equations, resulting

$$\begin{pmatrix} W_x \\ W_z \end{pmatrix} = (\underset{\sim}{\mathbf{M}}^T \underset{\sim}{\mathbf{M}})^{-1} \underset{\sim}{\mathbf{M}}^T \boldsymbol{d}. \tag{9}$$

However, the normal equations may have undesirable features with respect to numerical stability because the condition number of $\underset{\sim}{\mathbf{M}}^T\underset{\sim}{\mathbf{M}}$ is the square of the condition number of $\underset{\sim}{\mathbf{M}}$. If $\underset{\sim}{\mathbf{M}}$ is only moderately ill-conditioned, $\underset{\sim}{\mathbf{M}}^T\underset{\sim}{\mathbf{M}}$ is severely ill-conditioned. For this reason, methods that do not amplify the condition number

of $\underset{\sim}{\mathbf{M}}$ should be used to solve systems like (8) (for example QR factorization, Gill at al., 1990).

For estimating $W_x$ and $W_z$ *simultaneously* and *accurately*, $\underset{\sim}{\mathbf{M}}$ has to be well conditioned. Note that this is not the case when most of the elements of the matrix satisfy either $\Delta x_i^2 \gg \Delta z_i^2$ or $\Delta z_i^2 \gg \Delta x_i^2$. These two conditions describe cases when rays are traveling close to the horizontal or the vertical. In such cases, it is impossible to determine simultaneously both components of the vector $\boldsymbol{S}$ because of the limited view of the measurements translates immediately into severe ill-conditioning. This can be understood by trying to estimate $W_x$ and $W_z$ from the simple cross-well experiment shown in Figure 2, where $\Delta x^2 \gg \Delta z_i^2$. In this case

$$\underset{\sim}{\mathbf{M}} = \begin{pmatrix} \Delta x^2 & \Delta z_1^2 \\ \Delta x^2 & \Delta z_2^2 \end{pmatrix}.$$

The eigenvalues of this matrix are

$$\lambda_{\pm} = \frac{\Delta x^2 + \Delta z_2^2 \pm \sqrt{(\Delta x^2 - \Delta z_2^2)^2 + 4\Delta x^2 \Delta z_1^2}}{2}.$$

Because $\Delta x^2 \gg \Delta z_i^2$, the eigenvalues are approximately

$$\lambda_+ = \Delta x^2$$
$$\lambda_- = 0.$$

In other words, the smallest eigenvalue (zero in this case) is related to the vertical component of the slowness whereas the largest one is related to the horizontal component. On the contrary, for a VSP-like geometry largest eigenvalue is related to $S_z$ and the smallest one is related to $S_x$ (Dellinger, 1989). Having more rays ($M$) without increasing the aperture does not solve the problem. In such a case, the largest eigenvalue of the matrix ($\underset{\sim}{\mathbf{M}}^T \underset{\sim}{\mathbf{M}}$) tends to $\sum_{i=1}^{M} \Delta x_i^4$ and the smallest one tends to zero again.

The previous inversion scheme for homogeneous models can be generalized for estimating $\boldsymbol{S}$ in an heterogeneous medium. All we have to do is to solve systems of equations like (8) at each cell. In other words, the problem in the heterogeneous model is separated into many subproblems in homogeneous models. This approach might be easily implemented when the ray paths are used as basis functions for describing the slowness (Harris et al., 1990a) if, instead of averaging the slownesses of the different rays where they intersect, system of equations like (8) are solved to estimate the two components of the slowness.

Although this idea will not be exploited in the present paper, it can help us to understand *intuitively* which components of the slowness vector $\boldsymbol{S}$ are easier (or more difficult) to estimate from cross-well traveltimes measurements. In general, vertical variations in the medium are easier to estimate than horizontal variations. Vertical variations correspond to singular vectors associated with the largest singular values

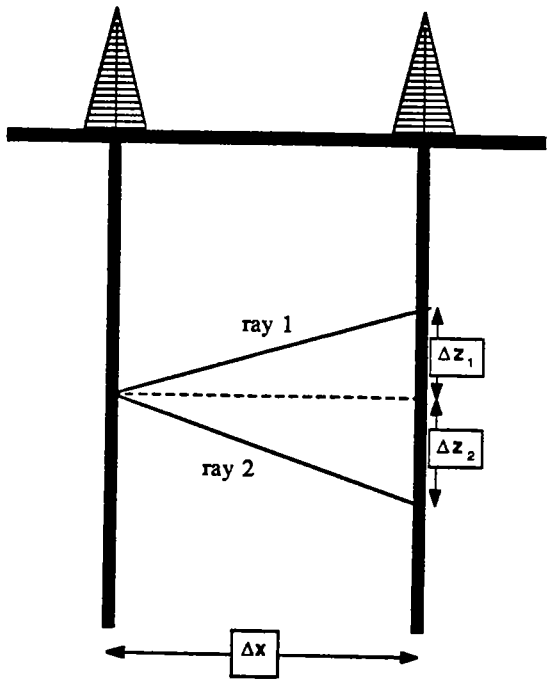


Figure 2: Cross-well experiment with two rays. (experiment) [R]

of the problem whereas lateral variations are associated to the smallest singular values (Pratt and Chapman, 1990). As explained earlier, in homogeneous models $S_x$ is related to the larger singular value and $S_z$ is related to the smaller one. Therefore, if the problem in a heterogeneous model is solved as many separate subproblems in homogeneous models, the largest singular values will be related to vertical variations in $S_x$ and the smallest ones will be related to lateral variations in $S_z$. We will demonstrate in the field data example that estimating horizontal variations in $S_z$ is indeed a difficult problem whereas it is always easier to estimate vertical variations in $S_x$.

Equation (5) can be used to estimate $\boldsymbol{S}$ for *all* the cells at the same time (rather than in a cell-by-cell basis, as explained before). This equation is obviously non-linear in $S_j$ and $S_{j+N}$. One way to solve the problem is by a sequence of linearized steps. We start by approximating (5) by a first order Taylor series expansion centered in a given model $\boldsymbol{S}_o$:

$$\begin{aligned} t_i(\boldsymbol{S}) &\approx t_i(\boldsymbol{S}_o) + \nabla t_i(\boldsymbol{S}_o) \cdot (\boldsymbol{S} - \boldsymbol{S}_o) \\ &= t_i(\boldsymbol{S}_o) + \sum_{j=1}^{N} \underset{\sim}{\mathbf{J}}_{ij} (S_j - S_{0j}) \end{aligned} \tag{10}$$

where the elements of the Jacobian $\underset{\sim}{\mathbf{J}}_{ij}$ are

$$\underset{\sim}{\mathbf{J}}_{ij} = \frac{\partial t_{ij}(\boldsymbol{S}_o)}{\partial S_j} = \begin{cases} \frac{\Delta x_{ij}^2 S_{0j}}{t_{ij}} & \text{if } 1 \leq j \leq N \\ \frac{\Delta z_{ij}^2 S_{0j}}{t_{ij}} & \text{if } N+1 \leq j \leq 2N \end{cases}$$

and $t_{ij}$ is the traveltime of the $i^{th}$ ray in the $j^{th}$ cell of the model $\boldsymbol{S}_o$ (equation (2)). If we assume that $t_i(\boldsymbol{S})$ represents one component of the vector of measured traveltimes, we can compute the perturbations $\Delta \boldsymbol{S}_j = (S_j - S_{oj})$ once the traveltimes in the reference model $\boldsymbol{S}_o$ has been calculated. The perturbation $\Delta \boldsymbol{S} = (\boldsymbol{S} - \boldsymbol{S}_o)$ is the solution of the following system of equations

$$\underset{\sim}{\mathbf{J}}\, \Delta \boldsymbol{S} = \Delta \boldsymbol{t} \tag{11}$$

where $\Delta \boldsymbol{t}_i = t_i(\boldsymbol{S}) - t_i(\boldsymbol{S}_o)$.

Note that the matrix $\underset{\sim}{\mathbf{J}}$ depends *explicitly* on the slowness of the reference model $\boldsymbol{S}_o$ in contrast with the isotropic case where the matrix depends only on the lengths of the rays in each pixel. In the isotropic case if the rays are straight, the estimation of the slowness becomes a linear problem because $\underset{\sim}{\mathbf{J}}$ is a constant. In the anisotropic case, however, the problem is still non-linear even if the rays are straight. Ray bending introduces another source of non-linearity.

In the examples shown later, equation (11) will be solved using the LSQR variant of the conjugate gradients algorithm (Nolet, 1987). We will show that by doing a few iterations with this method at each linearized step, the ill-conditioning of $\underset{\sim}{\mathbf{J}}$ caused by the limited view of the measurements is better handled than by solving the normal equations (in the overdetermined case).

## Meaning of the Results

Isotropic tomography fits circles ($t^2 = (x^2 + z^2)S^2$) to the data. Anisotropic tomography fits ellipses ($t^2 = x^2 S_x^2 + z^2 S_z^2$). Depending on the range of ray angles available (or the geometry used) and the wave type under consideration, the estimated slownesses $S_x$ and $S_z$ may or may not correspond to the real slownesses of the medium.

Horizontal or near horizontal rays are typical of a cross-well geometry. These rays sample a portion of the slowness surface close to the horizontal and for this reason the estimated $S_x$ corresponds to the real horizontal slowness. On the contrary, $S_z$ is not sampled by cross-well geometries. The inversion gives the vertical slowness of the best fitting ellipse ($S_{znmo}$) which coincides with the real vertical slowness only if the wave type considered is $SH$. However, we can generally expect $S_{znmo}$ to be closer than $S$ to the real vertical slowness. This will be illustrated later with field data by comparing $S$, $S_x$ and $S_{znmo}$ with sonic logs.

Vertical or near vertical rays are typical of a VSP-like geometry. From this type of geometry we can get $S_{xnmo}$ and $S_z$. These two slownesses plus $S_x$ and $S_{znmo}$ obtained

from cross-well geometries can be used to estimate the real slowness surface of the medium $S(\phi)$ using the following approximate expression (Muir, 1990):

$$S(\phi) = \frac{M_x^3 c^6 + M_x x^2 (2M_z + M_{znmo}) c^4 s^2 + (2M_x + M_{xnmo}) c^2 s^4 + M_z^3 s^6}{(M_x c^2 + M_z s^2)^2}$$

where

$$\begin{aligned} M_x &= S_x^{-2} \\ M_z &= S_z^{-2} \\ M_{xnmo} &= S_{xnmo}^{-2} \\ M_{znmo} &= S_{znmo}^{-2} \\ c &= cos(\phi) \\ s &= sin(\phi) \\ \phi &= \text{angle from the horizontal.} \end{aligned}$$

This expression is called the double elliptic approximation. Dellinger and Muir (1991) demonstrate that this approximation accurately fits general transversely isotropic media.

In the cross-well geometry examples that follow, the estimated vertical slowness will be referred to as $S_z$ rather than $S_{znmo}$.

## SYNTHETIC EXAMPLES

### 1-D Inversion

In this section, we will apply the previous technique to the inversion of traveltimes for a cross-well geometry. Synthetic data were generated through the 1-D isotropic model shown in Figure 3, using a geometry of 17 sources and 17 receivers equally spaced at the source and receiver well respectively. If we plot the components of the slowness vector $\boldsymbol{S}$ (equation(4)) for this model, we obtain the profile shown at the right hand side of Figure 3. Both slowness components are identical because the model is isotropic. In this example, the slowness contrast between the background and the anomalous layer is small (1%) and therefore, the propagation of the energy can be safely modeled by straight ray paths.

We can constrain the inversion by allowing only vertical variations in the model if it is know a priori that the medium is layered. Doing this we eliminate instabilities and non-uniqueness in the inversion associated with lateral variations, remaining only those associated with the vertical component of the slowness, which is not sampled propperly by the recording geometry.

The image area was divided into 100 layers of equal thickness (8 ft). The inversion process has to estimate 200 parameters from 289 traveltimes. Figure 4 shows the

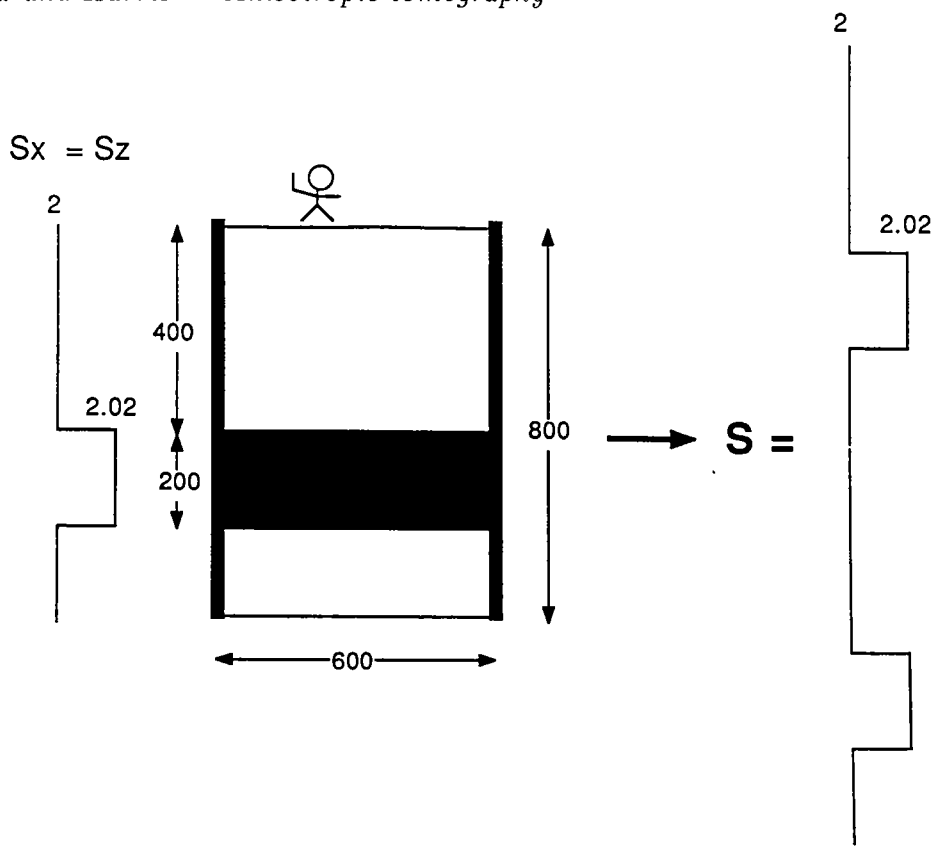


Figure 3: Synthetic isotropic model used to test the algorithm. At the right, it is shown the slowness vector $S$ that describes this model. (syn-model) [R]

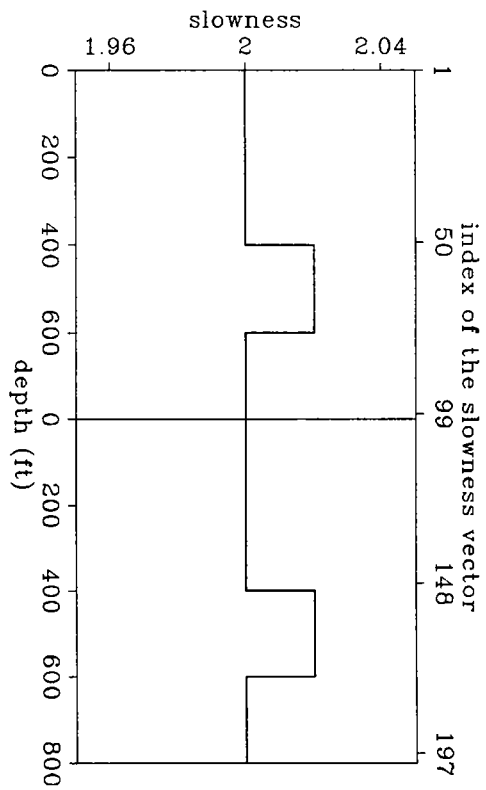


Figure 4: Result of the inversion of the synthetic data generated through the model shown in Figure 3. (1d-synthetic) [NR]

slowness vector obtained after 60 conjugate gradients (CG) iterations. There is no difference between the given $S$ (Figure 3) and the estimated one (Figure 4). Note also that the results can be represented as a function of depth as well as a function of the index of the slowness vector. In the two next results the depth axis will be omitted.

Figure 5 shows the convergence toward the result as a function of the CG-iterations. The result shown in Figure 4 correspond in Figure 5 to 60 CG-iterations in the axis *number of iterations*. The two "hills" represent the slowness at the anomalous layer. We say that convergence has been achieved when the top and the bottom of the hills are flat. Note that the horizontal component of the slowness converges faster than the vertical component. This is because in the given model, the horizontal component of the slowness in the anomalous layer is better sampled than the vertical component: the range of ray angles (absolute values) is from 0 to 53 degrees ($53 \approx \arctan(\frac{800}{600})$) which is a typical range for cross-well experiments.

If the same geometry is used to generate synthetic data through the model shown at the top of Figure 6 (were the well to well separation has been decreased), we obtain that both components converge at the same rate. This is because the vertical component of the slowness is better sampled than before: the range of ray angles varies between 0 and 76 degrees ($76 \approx \arctan(\frac{800}{200})$).

The previous results tell us that if it is not possible to perform "enough" iterations in order to reach the flat top of both hills ( Figures 5 and 6), we may wrongly conclude that the medium is anisotropic. What is really happening is that the components of the slowness vector do not converge at the same rate. Severe limited view problems as well as low signal to noise ratio are some reasons that may limit the amount of CG-iterations that can be performed before the ill-conditioning of the problem starts playing any role.

## 2-D Inversion

To test the performance of the algorithm in inverting data generated in a 2-D medium, we computed synthetic traveltimes through the isotropic model shown in Figure 7. The separation between contiguous sources and receivers is 10 ft and for each receiver gather, only sources located at $\pm 50$ degrees are used. With a geometry like this, we pretend to simulate the geometry of the real data example to be analyzed later. As in the 1-D example, the slowness contrast between the anomaly and the background is small (5%), and therefore, straight rays can be used again.

The unknown model was discretized in 241 x 46 pixels (5 $ft^2$) and therefore, the inversion has to estimate 241 x 46 x 2 parameters from 2200 synthetic traveltimes. Figure 8 shows the results of the inversion. The slowness of the isotropic circular anomaly (1.05) is better estimated by the horizontal than by the vertical component of the slowness. Remember that this is not the case in the 1-D inversion, where both slowness components can be perfectly recovered even thought the vertical component of the slowness is not properly sampled. The extra information introduced in that

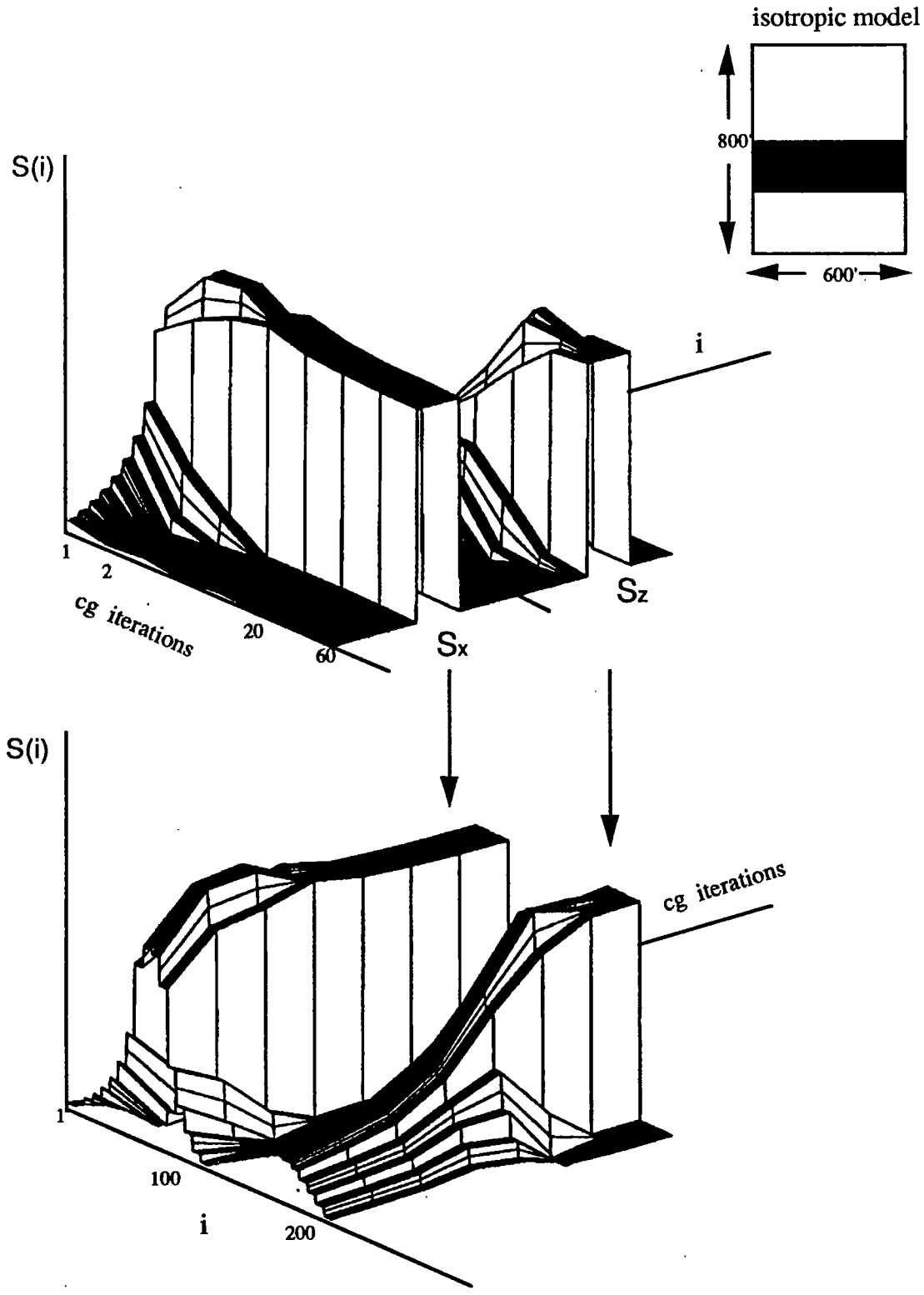


Figure 5: Variations of the slowness vector as a function of the number of conjugate gradient iterations. The original model is shown at the top. The axes "$i$" and "CG iterations" have been interchanged from one plot to the other. (cg-600x800) [R]

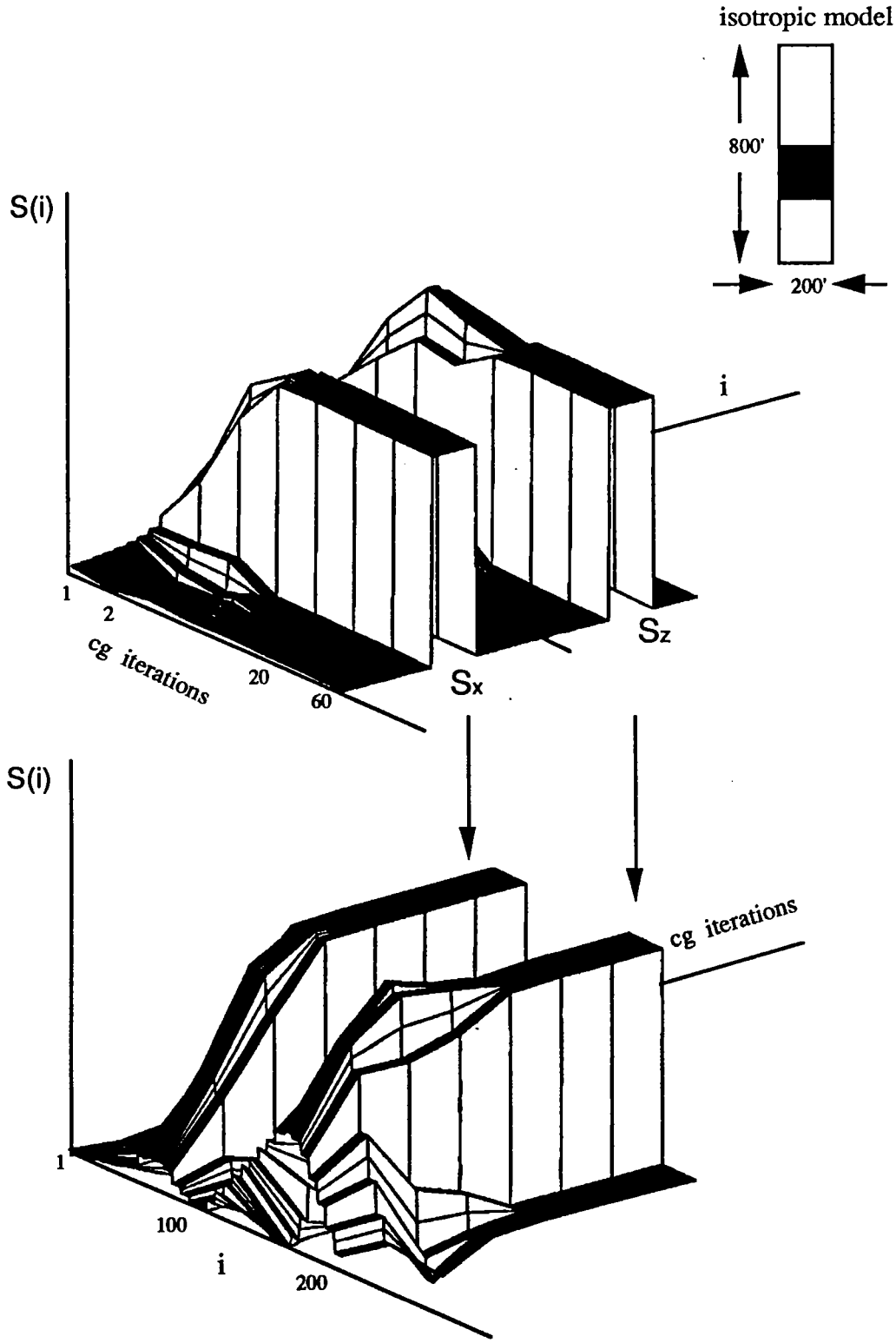


Figure 6: Variations of the slowness vector as a function of the number of conjugate gradient iterations. The only difference between the model shown at the top and the model of Figure 3 is in the horizontal dimension. The axes "*i*" and "CG iterations" have been interchanged from one plot to the other. (cg-200x800) [R]

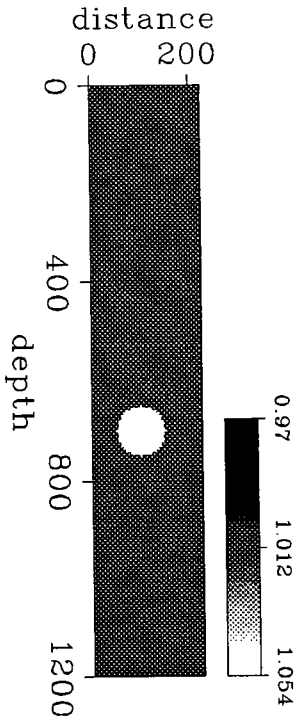


Figure 7: Isotropic slowness model. The radius of the circular anomaly is $r = 50$ and is centered at $(100, 700)$. The background slowness is 1.0 and the slowness of the disc is 1.05. (s-model-test) [NR]

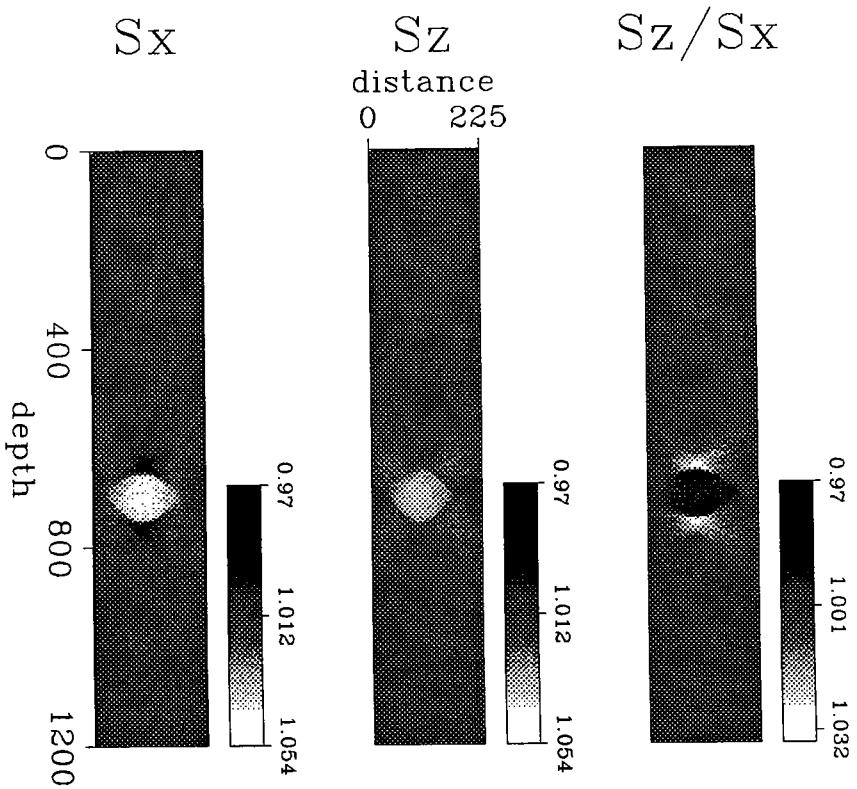


Figure 8: Reconstructed horizontal and vertical component of the slowness. The ratio of the two components is shown at the right. (sx2d-test) [NR]

problem by assuming that the model is layered compensates for the limited view of the measurements. In the 2-D inversion, where the unknown is less constrained, the better sampling of the horizontal component translates into a better recovery of that component and as a result, some artificial anisotropy is introduced by the reconstruction. In this noise-free example such an anisotropy is not greater than 3% as shown in Figure 8 by the ratio $\frac{S_z}{S_x}$. Doing more CG-iterations does not help to reduce this artificial anisotropy to zero, like in the 1-D inversion (Figures 5 and 6). In the present case the images didn't change after 120-CG iterations.

The artifacts in both slowness components are similar to the well known truncation artifacts in isotropic inversion although they are different from one component to the other. The estimated $S_x$ is smeared along the horizontal direction whereas $S_z$ is not. This is because the estimation of $S_z$ is not affected by rays that travel horizontally. The different character of the artifacts for each slowness component can limit our ability to recover variations in anisotropy at the same scale of variations in velocity when data from only one geometry is used. This will be clearly observed later in the application to field data.

## FIELD DATA EXAMPLE

Anisotropic tomography was performed using a field data set. This data set was acquired jointly by Amoco and Stanford University at the Gulf Coast, on shore, in Southeast Texas. The overall survey geometry is illustrated in Figure 9, and it is similar to the one used in the synthetic example of 2-D inversion. More details about the site and geometry are found in Harris et al. (1990b).

Nearly 5000 $P$-wave first arrival times were picked from the data. In general, we found that the traveltimes corresponding to the near horizontal rays (near offsets) were more difficult to pick than those at far offsets.

### Well Deviation

In this particular geometry, the wells are not confined to a single plane. Instead, they deviate gradually form the vertical plane that contains both wells at the near surface. We have taken this effect into account following this two-steps procedure:

- Find the true 3-D distances between sources and receivers.
- Assume that one well is vertical (for example, the source well) and locate the receivers at the corresponding real distances and real depths in the other well. This is equivalent to locate the origin of the coordinates to measure the distances always at the source well.

When correcting for the well deviation in this way, true source-receiver separations are used in the inversion. The relative position of the two wells after considering the

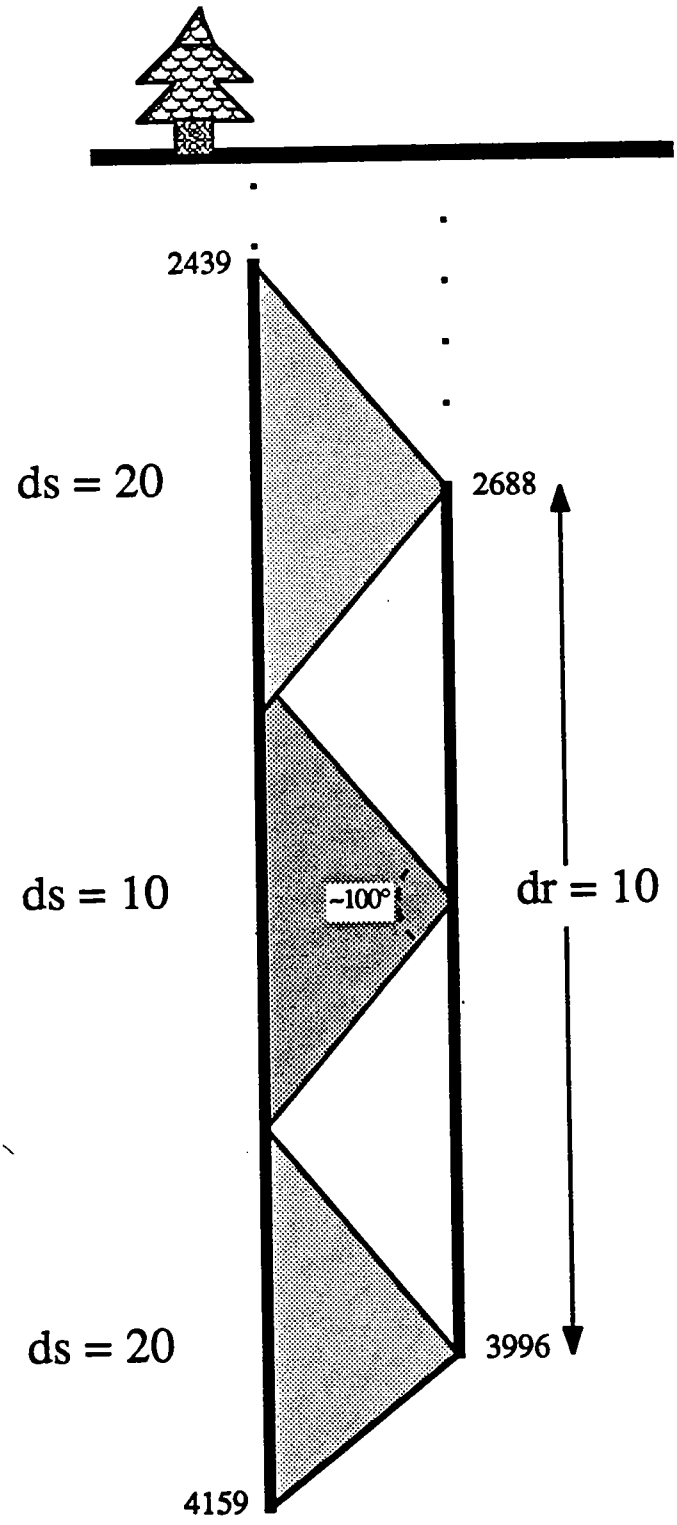


Figure 9: Overall survey geometry illustrating the shooting pattern. Receivers are spaced at $dr = 10$ ft between 2688 and 3996 ft Sources are spaced at $ds = 10$ ft interval in primary target zone and $ds = 20$ ft. above and bellow the target zone. The average separation between wells is 225 ft. (geometry) [R]

deviation is shown in Figure 10. To use the true distances, it is necessary to move the receivers positions horizontally in the deviated well. This is way the receiver positions in Figure 10 look like horizontally smeared. The selection of the vertical well used as a reference to measure the relative deviations is irrelevant if we assume that the model is 1-D. In 2-D somewhat different distorsions may occur depending on which well is chosen as a reference.

1-D Inversion

The simplest inversion that we can possibly do is assuming that the medium is homogeneous isotropic. What we obtain is the mean velocity (equation (7)), in this case $V_{iso} = 8452$ ft/sec. The next step is to assume that the model is still homogeneous but elliptically anisotropic. Using equation (8) we find that $V_x = 8586$ ft/sec and $V_z = 8079$ ft/sec. Notice that for this particular recording geometry (Figure 9), $V_{iso}$ is closer to $V_x$ than to $V_z$, which means that the "averaging" of the horizontal and vertical directions that the isotropic inversion implicitly does is not a simple arithmetic average. When the model is also heterogeneous, the same conclusion may be drawn as it will be show later.

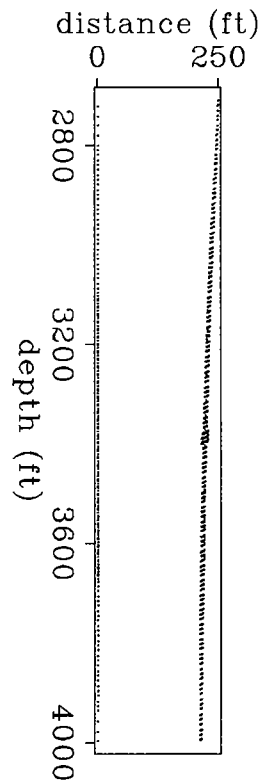


Figure 10: Positions of the source and receiver wells after considering their relative deviations. Each dot represents a source or a receiver position (left and right respectively). Note that the density of sources is larger at the middle of the surveyed area than in the extremes. (deviation) [NR]

To measure the goodness of the fit between measured and calculated traveltimes, we use the mean-absolute value of the mismatch

$$error = \frac{1}{M}\sum_{i=1}^{M}|t_{c_i} - t_{r_i}|, \tag{12}$$

where $t_{r_i}$ and $t_{c_i}$ are the measured and calculated traveltimes respectively and $M$ is the total number of traveltimes.

When the estimated $V_{iso}$ in the homogeneous model is used to compute synthetic traveltimes, $error$ = 1.04 ms. When the model is homogeneous anisotropic, $error$ = 0.94 ms.

The result of the isotropic inversion assuming a layered medium is shown in Figure 11. Only traveltimes corresponding to rays below 2705 ft and above 4000 ft were used. This depth interval was discretized in 60 horizontal layers of equal thickness (21.583 ft). Straight rays were used to compute synthetic traveltimes since small velocity variations are expected in this site (Harris et al., 1990b). Conjugate gradients iterations (40) were performed until no appreciable changes were seen neither in the model nor in the mean-absolute value of the error (equation (12)). This corresponds to reaching the flat part of the hills in Figure (5). For the model shown in Figure 11, $error$ = 0.67 ms.

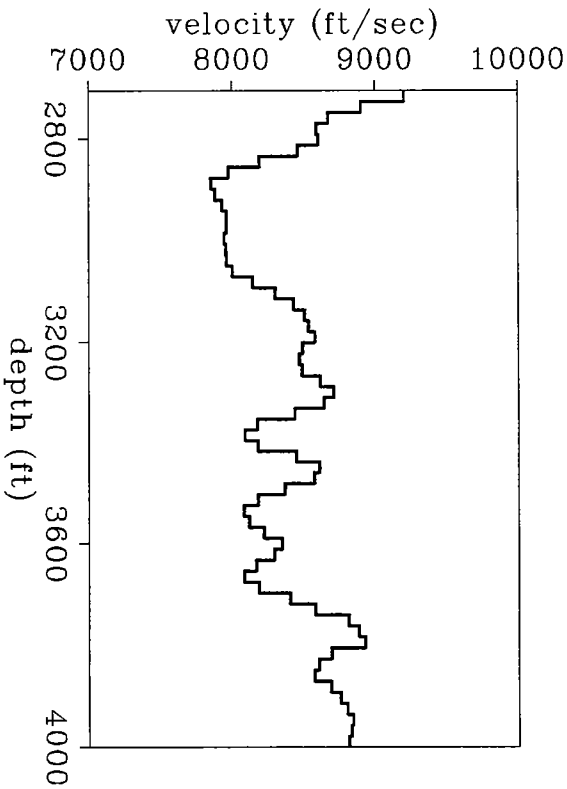


Figure 11: Result of the isotropic layered inversion. The thickness of each layer is 21.583 ft (Isos) [NR]

Now, we allow the model to be anisotropic. The result of the inversion is shown in Figure 12. For traveltimes computed through this model, *error* = 0.59 ms. The thick curve represents the horizontal velocity and the thin one represents the vertical velocity. The first thing we notice is that as expected $V_x$ is generally larger than $V_z$. Figure 13 compares $V_x$ and $V_z$ with $V_{iso}$. In general, $V_{iso}$ is closer to $V_x$ than it is to $V_z$, which is consistent with the previous the results of the inversion assuming an homogeneous medium. This means that for the type of recording geometry used (ray angles between 0 and ±50 degrees) the isotropic inversion is affected primarily by the horizontal component of the velocity. Since there are fewer rays at large angles, the isotropic inversion is less constrained by them. However, rays at large angles contain independent information that might be important to improve horizontal resolution in 2-D models.

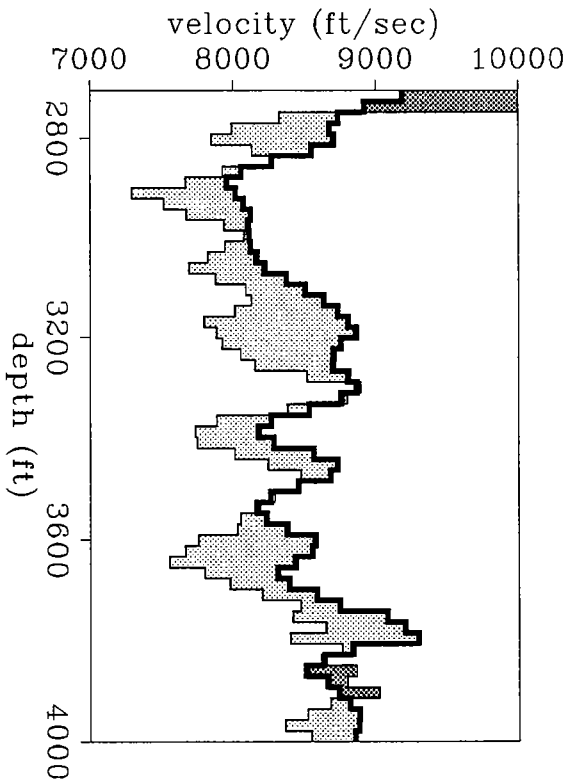


Figure 12: Result of the anisotropic layered inversion. The thickness of each layer in 21.583 ft The differences between $V_x$ (thick line) and $V_z$ (thin line) are represented by two colors: light gray, when $V_x > V_z$ and dark gray when $V_x < V_z$. (Anisxsz) [NR]

Sonic logs were available in this site at both wells (Figure 14). They sample the vertical velocity about the well at frequencies ($\sim$ 10 kHz) much larger than the typical frequency of the cross-well data ($\sim$ 1 kHz). To compare the information obtained from this two types of measurements (1-D tomogram and velocity logs), we did some averaging to the logs. First, we averaged each slowness log in blocks of equal thickness and equal to the layer thickness in the 1-D tomographic inversion. Secondly, the two averaged slowness logs were averaged again into a single one. The purpose of the last averaging was to simulate the horizontal averaging that the 1-D

tomographic inversion implicitly does. Figure 15 compares the average velocity log with $V_{iso}$, $V_x$ and $V_z$. Note that $V_z$ is not only much closer to the average velocity log (as expected) but also better correlated with it, when compared with $V_{iso}$ and $V_x$.

The ratio $V_x/V_z$ is a lithologic indicator as shown in Figure 16. In this figure, the thick line corresponds to the ratio $V_x/V_z$ and the thin one corresponds to the average spontaneous potential (SP) log. The average SP log was obtained by blocking each log separately, taking the average of the results and removing a linear trend with depth in the final average. Notice the good correlation between large SP values (shales) and large anisotropy ratio. The same for low SP values (sands) and isotropic layers. The differences between the shape of the two curves are because 2D-variations in the true medium are averaged out in the 1-D inversion as well as in the average SP log. The 2D nature of the true medium will be seen clearly later when performing 2D inversion.

In the anisotropic inversion, we found that for this particular data set 60 layers of 21.583 ft each was a good compromise between resolution and stability. Reducing the layer thickness by half has the effect (not shown) of increasing the resolution at the expense of large variations and instabilities in the vertical component of the velocity that is not well sampled by the recording geometry. The horizontal component of

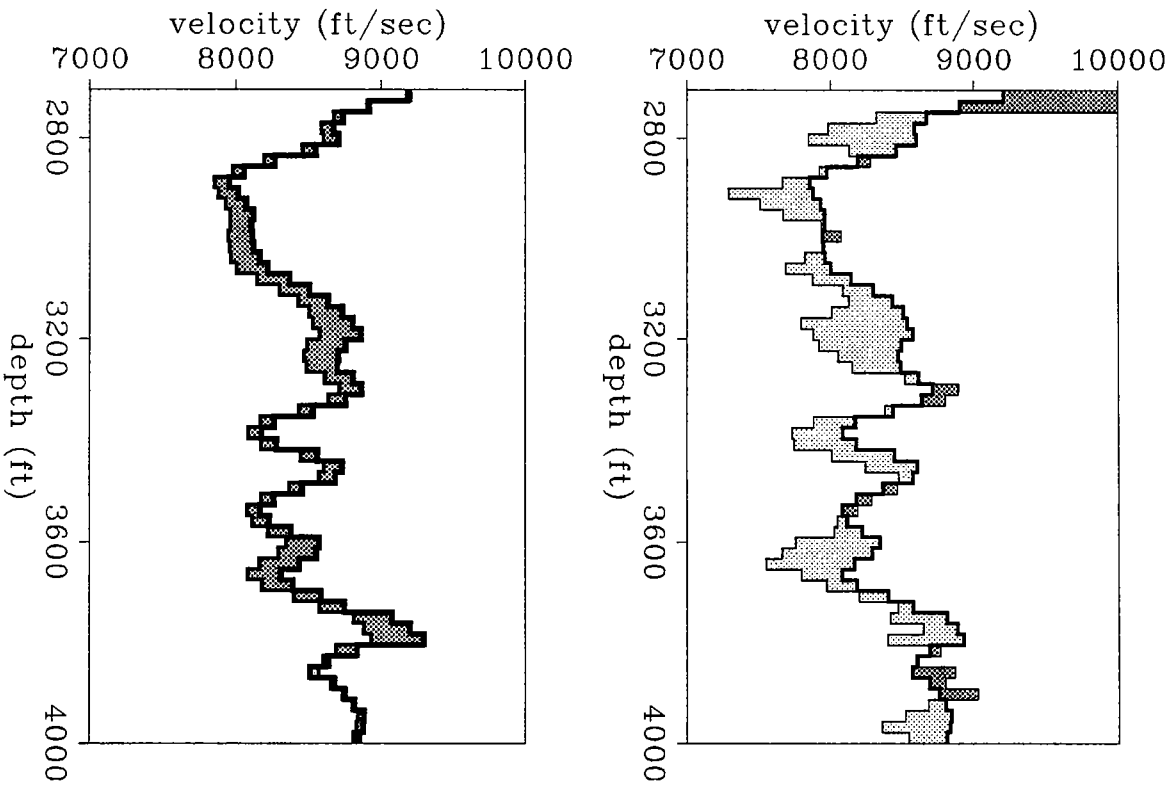


Figure 13: Comparison between isotropic and anisotropic layered inversion. Left: $V_{iso}$ (thin line) and and $V_x$ (thick line). Right: $V_{iso}$ (thick line) and $V_z$ (thin line). The differences between the isotropic and anisotropic inversion are represented by two colors: light gray when $V_{iso} > V_x$ or $V_z$, and dark gray when $V_{iso} < V_x$ or $V_z$. (IsosAnisxsz) [NR]

velocity is generally more stable than the vertical for smaller layer thicknesses. Obviously, increasing the layer thickness made the inversion more stable at the expense of less resolution.

## 2-D Inversion

When the problem is linear we should obtain the model that "best" fit the data in only one iteration. When the problem is non-linear one approach is to solve it as a sequence of linearized steps. We usually call these steps *external* iterations, to differentiate them from the *internal* iterations needed to solve each linear problem when using iterative techniques such as conjugate gradients. Ideally, if the problem has $n$ unknowns, each external iteration should consists of $m$ CG-steps ($m$ internal iterations), where $m \leq n$ is the number of different singular values. When dealing with field data, however, we might not be able to do this because of the presence of the noise. Noise can affect the solution of each linearized problem in the following ways: (a) It might be amplified in the model by the smallest singular values recovered when $m$ iterations are performed, (b) It might affect considerably the accuracy of the search directions and consequently, the position of the minimum associated with the solution. Therefore, we have to deal carefully with the noise.

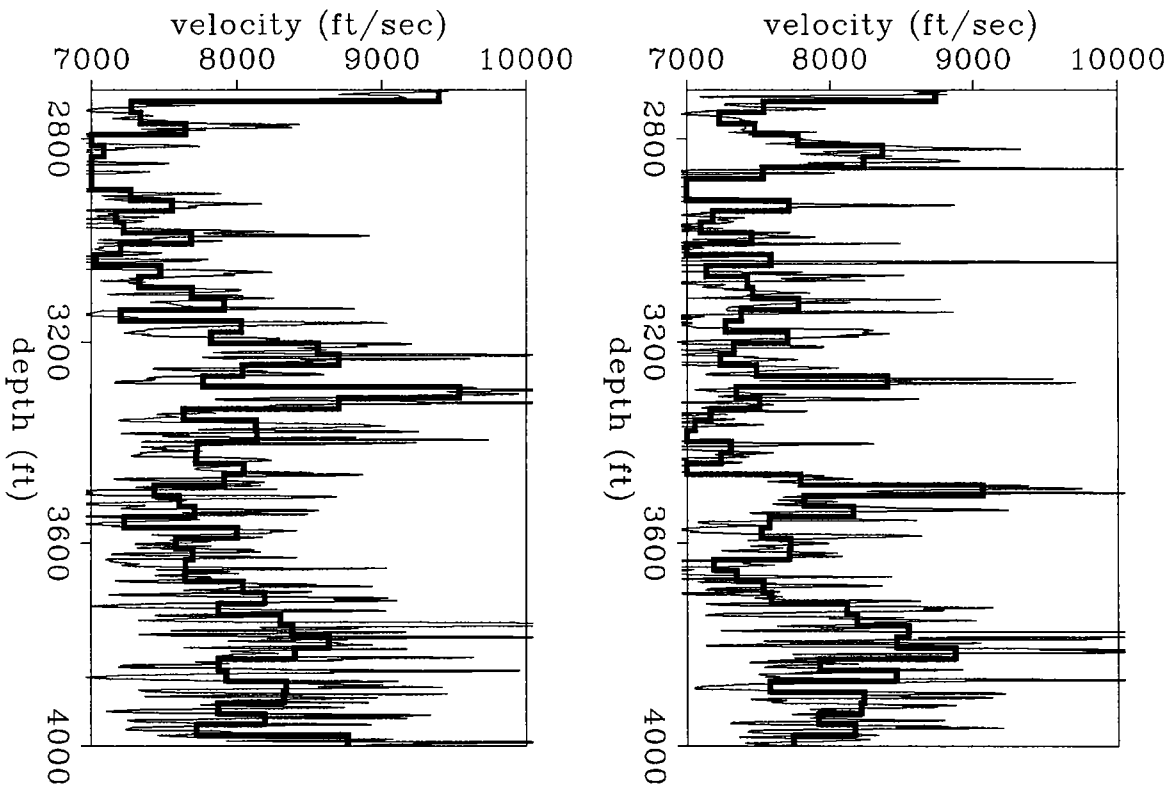


Figure 14: Sonic logs at the source and receiver well respectively. The thin line represents the original log. The thick line represents the corresponding log averaged in 60 layers of equal thickness (21.583 ft) (two-logs) [NR]

Under the straight-ray assumption, only one external iteration was needed in the 1-D inversion to find the model shown in Figure 12. By selecting the layer thickness appropriately, we were able to perform the CG-iterations required to reach convergency without being much affected by the noise: thicker layers damped the solution whereas thiner layers introduced instabilities. In 2-D, however, the situation is different. In this case we found that the results were more sensitive to noise in the data than 1-D results. This is not surprising because now we are trying to estimate horizontal variations in $S_z$ which, as explained before, are related to the smallest singular values of the problem (that amplify the noise).

Because of the sensitiveness to the noise of the 2-D inversion, it is necessary to avoid "many" CG-iterations at each linearized step. After several tests combining in different ways external and internal iterations with mean-average smoothing of the slowness model, we adopted a conservative approach to minimize the error (12). The approach consisted of the following steps: (1) Compute traveltimes in the given model, calculate the matrix $\underset{\sim}{\mathbf{J}}$ and find the residuals. (2) Approximate the solution of the linear problem (11) by applying few (typically one or two) CG-iterations. (3) Smooth the updated slowness model. (4) Repeat all the previous steps until there is no reduction in the sum (12). When this happens, either quit or increase the number of CG-iterations by one and check if further reductions in the mismatch are obtained. If the problem is linear, the solution is not obtained in only one iteration because of the presence of the noise.

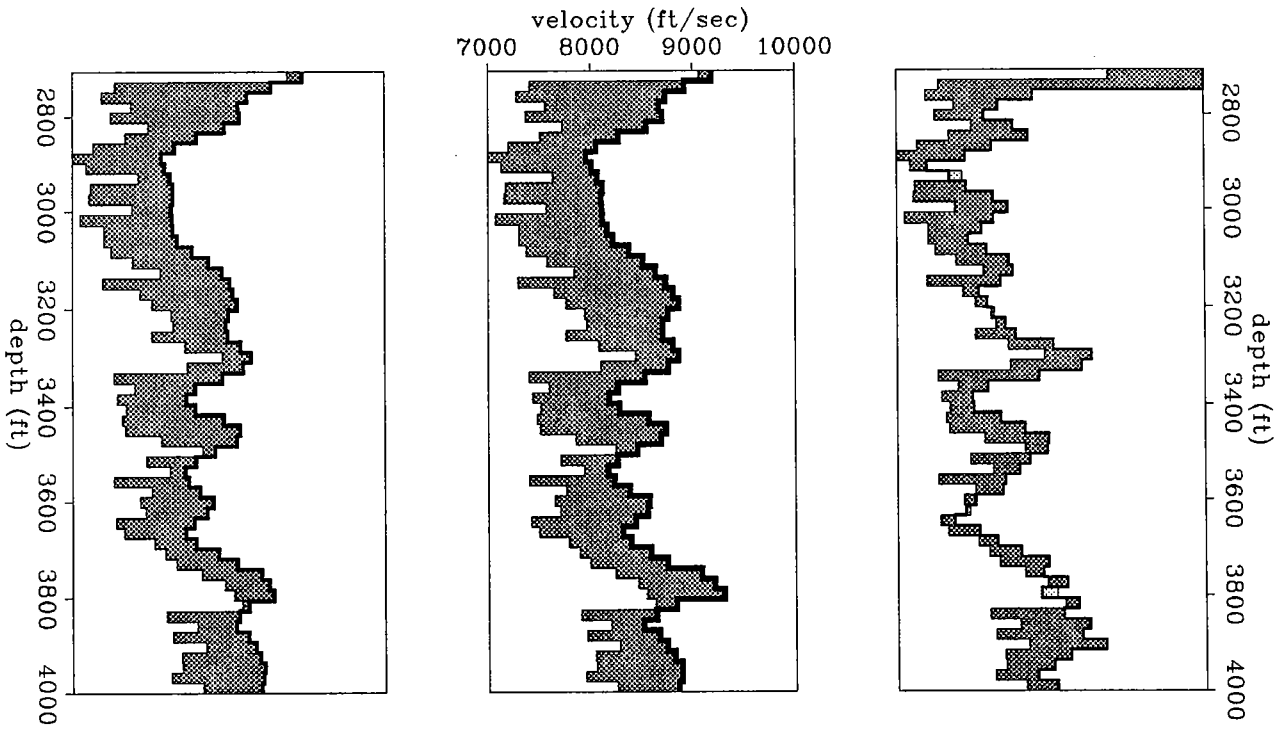


Figure 15: Average velocity log compared with $V_{iso}$ (left), $V_x$ (center) and $V_z$ (right). $V_z$ is closer and better correlated with the velocity log. (logs-vs-veloc) [NR]

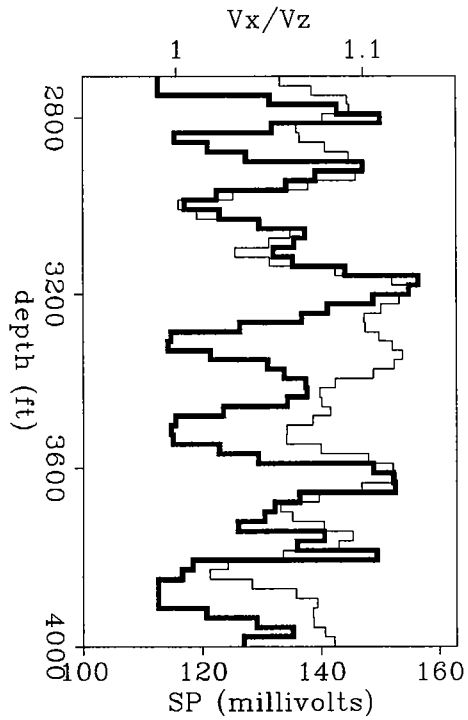


Figure 16: Anisotropy ratio $V_x/V_z$ (thick line) compared with the SP log (thin line). (SP-Ani) [NR]

When the previous procedure was applied to estimate an isotropic model from the data, we obtained the image shown in Figure 17 (*error* = 0.54 ms). In this case, the unknown model was discretized into 131 x 26 square cells (10 ft$^2$ each). It is interesting to notice that adding more degrees of freedom in structure (more cells) does not improve substantially the parameter *error* obtained with 28 times less degrees of freedom in the 1-D anisotropic inversion. The model shown in Figure 17 is similar to the one obtained by Harris et al. (1990b).

The result of the anisotropic inversion is shown in Figure 18 (*error* = 0.45 ms). Notice that $V_x$ is remarkably similar to $V_{iso}$, like in the 1-D inversion. The main difference between these two images is that in $V_x$ (Figure 18) the events tend to be more horizontally smeared that in $V_{iso}$ (Figure 17). This was expected from the synthetic example shown in Figure 8.

The events in the vertical component of the velocity tend to be smeared in the direction of the steepest rays and the spatial resolution in this component is poor when compared with $V_{iso}$ and $V_x$. This is because $V_z$ is not properly sampled by the recording geometry. In the 1-D case, as we said before, this lack of information is compensated by assuming a layered model, which allows to perform more CG-iterations without having problems with the noise. In 2-D this is not possible and therefore, the results obtained can be in a stage where $V_x$ is close to convergency but $V_z$ is far from that point. This in turn introduces artificial anisotropy.

Because $V_x$ and $V_z$ cannot be estimated at the same resolution (at least using only this type of recording geometry), it is not possible to estimate spatial variations in velocity anisotropy (the ratio $V_x/V_z$ for example) at the same scale of the variations in velocity. Still, an image that shows variations in velocity anisotropy can be useful if it accounts only for the large scale variations that are well resolved by the inversion. Such an image is shown in Figure 18. This image is divided into four areas: highly anisotropic, moderately anisotropic, isotropic and anisotropic with $V_z > V_x$. We can see that most of the model is isotropic whereas the anisotropic areas are associated with high isotropic-velocity zones, possibly shales.

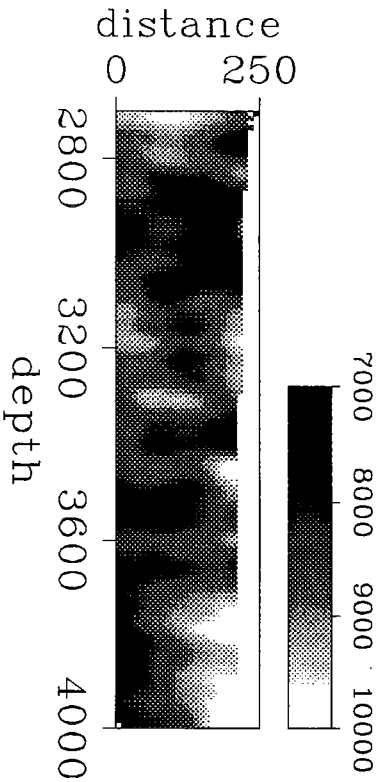


Figure 17: Isotropic 2-D inversion. The image has been divided into 131 x 26 square cells (10 ft$^2$ each). (s2d-iso-hast) [NR]

The mismatch estimated by equation (12) (*error*) decreases roughly 50% from the homogeneous to the 1-D inversion and about 60% from the homogeneous to the 2-D inversion. This means that for this data set, by trying to estimate lateral variations in the medium (small singular values) only a 10% reduction in the mismatch is gained with respect to estimating *only* vertical variations in the model (largest singular values).

## Biases in the Inversion

The main problem considered in the previous sections was how the limited view of the measurements affect our ability to estimate velocities in different directions.

By assuming elliptic anisotropy it was necessary to estimate only two velocities: horizontal and vertical. Of course, this is too simple to describe the real complexities of the velocities in many cases but still, it is the first step beyond fitting the data with circles (isotropic tomography). We have seen that unless we constrain considerably the inversion (layered models) or we have measurements from a wide range of angles, it is difficult to estimate *accurately* and *simultaneously* $S_x$ and $S_z$. Unfortunately, even if these conditions are satisfied, many other factors may affect the results.

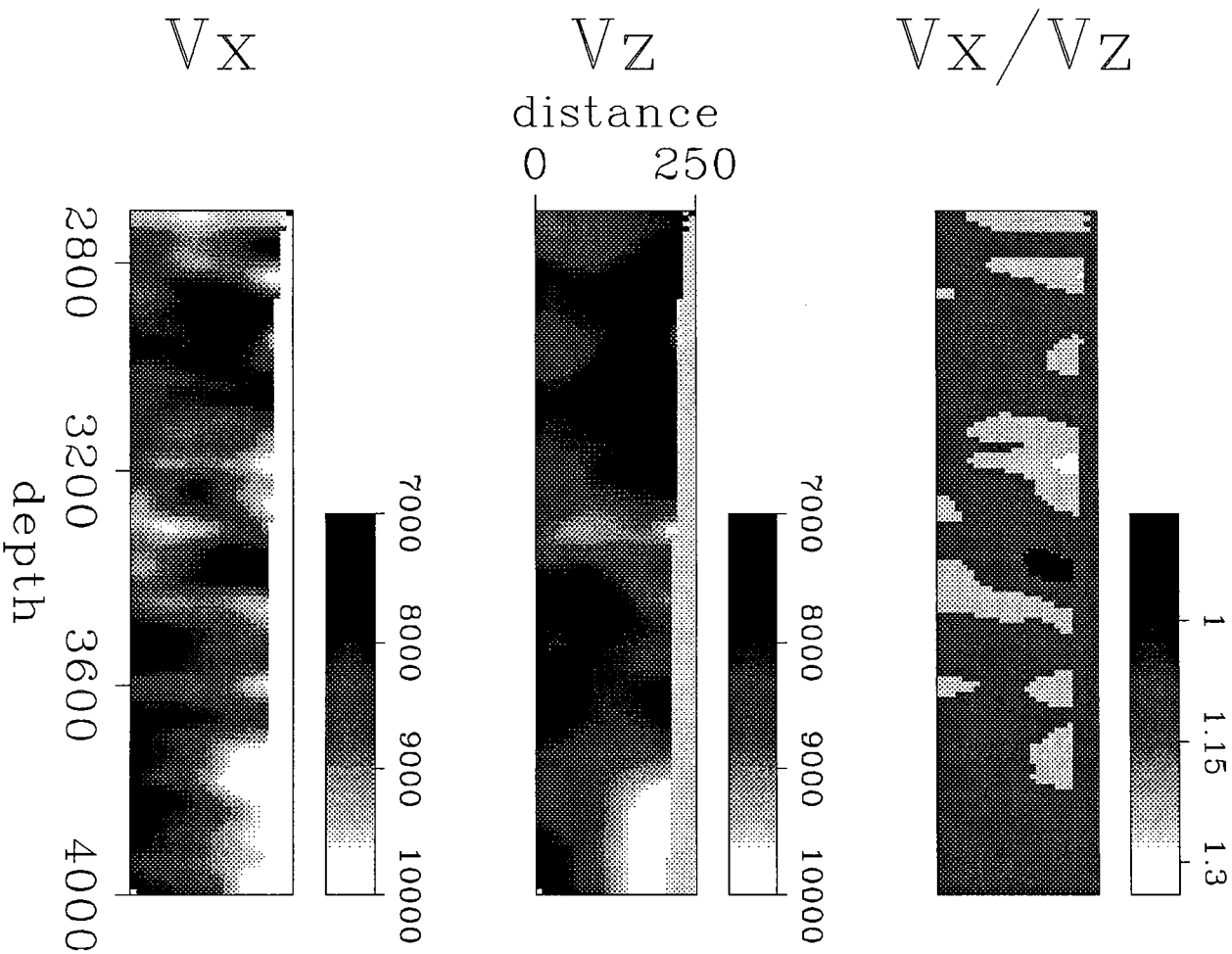


Figure 18: Anisotropic 2-D inversion. Each image has been divided into 131 x 26 square cells (10 ft$^2$ each). The spatial resolution of $V_z$ is poor when compared with the spatial resolution of $V_x$.The ratio $V_x/V_z$ has been separated in four areas that show percentages of anisotropy: white (ratio $>$ 1.25), light gray (1.06 $<$ ratio $\leq$ 1.25), dark gray (0.90 $<$ ratio $\leq$ 1.06) and black (ratio $\leq$ 0.9). The dark gray areas can be considered isotropic. (sx2d-hast) [NR]

Among this factors we have:

- Picking errors. These errors may increase or decrease systematically the velocities, depending on which part of the first arriving wavelet has been picked. Picking before the correct value speeds up velocities whereas picking later slows

them down. This may explain why in Figure 15 $V_z$ is systematically 1 or 2 % faster than the sonic log.

- Well deviation. As we said before, the wells deviate in 3-D but we decided to work in 2-D. If the real 3-D variations in the medium are moderate, this is a good approximation but it may not be otherwise. When first testing our algorithm with real data the well deviation was not considered. We just substituted each well by a vertical one located at its average surface location. The results were (not shown) higher velocities (than those shown in Figure 12) where the wells were actually closer and lower velocities where the wells were actually farther apart. Considering the well deviation affected $S_x$ more than $S_z$.

- Head waves vs. body waves. Although this may be considered a picking error, it affects primarily traveltimes at near offsets (small ray angles) in low velocity layers. These errors affect mainly the estimation of $S_x$ because $S_z$ does not use information from rays that travel at small angles. In principle, when head waves are inverted like body waves the estimated horizontal velocity turns out to be faster than the real one.

- Ray bending.

All the previous factors, when not considered appropriately, may produce artificially anisotropic results. For this reason and the ill-conditioning of the problem studied later, the estimation of small scale 2D variations in velocity anisotropy is a difficult task.

## CONCLUSIONS

We have presented the basic theory and examples of an algorithm that performs anisotropic traveltime tomography. The algorithm generalizes the well known techniques of tomographic traveltime inversion by using models discretized into a set of homogeneous, elliptically-anisotropic cells, where each cell is characterized by two slownesses, one vertical and the other horizontal. Both components of the slowness can be estimated simultaneously provided that the range of ray angles is great enough. Otherwise the problem becomes ill-conditioned. As expected for cross-well geometries, the ill-conditioning is more severe in the estimation of the vertical component of the slowness. This is another reason why we should combine information from different geometries (VSP, surface-to-surface, and cross-well), since taken alone they may have limited aperture.

## ACKNOWLEDGMENTS

We thank Francis Muir for many interesting discussions and important suggestions. We would like also to thank Amoco Production Company, the Gas Research

Institute and the Seismic Tomography Project at Stanford University for providing the data. The first author thanks INTEVEP, S.A. for financial support.

## REFERENCES

Byun, B. S., and Corrigan, D., 1990, Seismic traveltime inversion for transverse isotropy: Geophysics, **55**, 192-200.

Chapman, C. H. and Pratt, R. G., 1990, Traveltime tomography in anisotropic media: theory: submitted to Geophys. J. Intl.

Cunha-Filho, C. A., 1990, Traveltime inversion of a cross-well data set for elliptically anisotropic media: SEP-**67**, 31-40.

Dellinger, J., 1989, Anisotropic traveltime inversion with error bars: theory: SEP-**60**, 253-260.

Dellinger, J., and Muir, 1991, The double elliptic approximation in the group and phase domains: SEP-**70**, 361-366.

Gill, P. E., Murray, W., and Wright, M. H., 1991, Numerical lineal algebra and optimization, volume 1: Addison-Wesley Publishing Company.

Harris, J. M., Lazaratos, S., and Michelena, R., J., 1990, Tomographic string inversion: STP-**1**, Paper B.

Harris, J. M., Mavko, G., Moos, D., and Nolen-Hoeksema, R., J., 1990, Cross-well tomographic imaging in Gulf Coast sediments: STP-**1**, Paper A.

Karrenbach, M., 1989, Velocity and $Q$ in transverse isotropic media: SEP-**60**, 271-283.

Levin, F. K., The reflection, refraction, and diffraction of waves in media with elliptical velocity dependence: Geophysics, **43**, 528-537.

McMechan, G. A., 1983, Seismic tomography in boreholes: Geophys. J. Roy. Astr. Soc., **74**, 601-612.

Muir, F., 1990, A modified anisotropic system: SEP-**67**, 41-42.

Nolet, G., 1987, Seismic wave propagation and seismic tomography, *in* Nolet, G., Ed., Seismic tomography: D. Reidel Publ. Co., 1-23

Pratt, R. G., Chapman, C. H., 1990, Traveltime tomography in anisotropic media: application: submitted to Geophys. J. Intl.

White, J. E., Martineau-Nicoletis, L., and Monash, C., 1983, Measured anisotropy in Pierre shale: Geophys. Prosp., **31**, 707-725.

Winterstein, D. F., 1986, Anisotropy effects in $P$-wave and $SH$-wave stacking velocities contain information on lithology: Geophysics, **51**, 661-672.